Journal of Physics: Conference Series **674** (2016) 012014 doi:10.1088/1742-6596/674/1/012014

# Characterisation of irradiation-induced defects in ZnO single crystals

**I Prochazka[1] , J Cizek[1], F Lukac[1], O Melikhova[1], J Valenta[1], V Havranek[2], W Anwand[3], V A Skuratov[4] and T S Strukova[4]**

[1] Faculty of Mathematics and Physics, Charles University in Prague, V Holesovickach 2, CZ-180 00 Praha 8, Czech Republic
[2] Nuclear Physics Institute, Academy of Sciences of the Czech Republic, CZ-250 68 Husinec-Rez, Czech Republic
[3] Institute of Radiation Physics, Helmholtz-Zentrum Dresden-Rossendorf, Bautzner Landstr. 400, 01328 Dresden, Germany
[4] Flerov Laboratory of Nuclear Reactions, Joint Institute for Nuclear Research, 141 980 Dubna, Moscow region, Russian Federation

E-mail: ivan.prochazka@mff.cuni.cz

**Abstract**. Positron annihilation spectroscopy (PAS) combined with optical methods was employed for characterisation of defects in the hydrothermally grown ZnO single crystals irradiated by 167 MeV $Xe^{26+}$ ions to fluences ranged from $3\times10^{12}$ to $1\times10^{14}$ $cm^{-2}$. The positron lifetime (LT), Doppler broadening as well as slow-positron implantation spectroscopy (SPIS) techniques were involved. The *ab-initio* theoretical calculations were utilised for interpretation of LT results. The optical transmission and photoluminescence measurements were conducted, too. The virgin ZnO crystal exhibited a single component LT spectrum with a lifetime of 182 ps which is attributed to saturated positron trapping in Zn vacancies associated with hydrogen atoms unintentionally introduced into the crystal during the crystal growth. The Xe ion irradiated ZnO crystals have shown an additional component with a longer lifetime of ≈ 360 ps which comes from irradiation-induced larger defects equivalent in size to clusters of ≈ 10 to 12 vacancies. The concentrations of these clusters were estimated on the basis of combined LT and SPIS data. The PAS data were correlated with irradiation induced changes seen in the optical spectroscopy experiments.

## 1. Introduction

Zinc monoxide is a direct wide band gap semiconductor predestined for numerous applications: optoelectronic devices, transparent electrodes for solar cells, UV light emitting diodes and lasers, gas sensors *etc*. Application potential of ZnO origins from its large electronic band gap value of $E_g^{(el)} = 3.37$ eV as well as a large exciton binding energy of $E_x \approx 60$ meV at room temperature [1]. Moreover, high-quality bulk ZnO single crystals grown using the hydrothermal (HTG) or pressurised melt growth (MG) techniques have become readily available on the market. Progress in manufacturing the ZnO nanostructures and thin layers has further extended application area of zinc oxide [2].

It is well recognised [1] that functional properties of ZnO based materials, in particular, their optical and electrical features can be strongly influenced by impurity atoms and lattice defects. In this respect, the investigations of structure modifications induced in ZnO by ion implantations deserve attention. There are two main motivations for such investigations: (i) Material properties desired for

a particular application may be tailored in this way. (ii) Irradiation-induced degradation of the materials purposed for use in enhanced radiation conditions, *e.g.* in space applications, can be examined. Previous studies of irradiation effects on ZnO were concentrated mainly on the light-particle projectiles [3,4] or implantation of the light ions of energies ranging up to several MeV [5,6]. Information on structure changes induced in ZnO by irradiations with the energetic (≈ 100 MeV) heavy ions is yet rather scarce. To authors' knowledge, only the investigations of zinc oxide bulk crystals irradiated with 100 MeV oxygen and carbon ions [7] and ZnO nanostructured layers irradiated with 130 MeV $Xe^{23+}$ ions [8] have been reported so far. Scanning electron microscopy and optical methods were utilised in these two investigations. Among native impurities in ZnO, hydrogen has to be paid an attention in HTG crystals since H atoms can be easily incorporated into ZnO lattice [9] forming there a shallow donor state [10]. A complex of a zinc vacancy ($V_{Zn}$) with a H atom, denoted below as $V_{Zn}$–1H, has been clearly identified as a grown in defect in the HTG bulk ZnO crystals [9,11].

In the present Contribution, positron annihilation spectroscopy (PAS) was used to investigate lattice defects created in the ZnO bulk single crystals irradiated with energetic Xe ions at different fluences. The goal of this investigation was to characterise the irradiation induced defects on a level of atomic arrangement. The conventional PAS, *i.e.* the technique employing $\beta^+$ particles from a radionuclide source directly implanted into the sample, was utilised to measure positron lifetimes (LT) and Doppler broadening (DB) of annihilation radiation in its coincidence mode (CDB). In addition, slow-positron implantation spectroscopy (SPIS) with a monoenergetic positron beam was used for determination of positron diffusion lengths. In order to correlate the PAS results with irradiation induced changes in the optical properties of ZnO, two kinds of optical measurements were also performed: optical transmittance (OT) and photoluminescence (PL). A comparison of the present Xe implantation data with those obtained recently for ZnO crystals irradiated with 2.5 MeV protons was also made.

## 2. Experimental details

### *2.1. Zinc oxide samples*

In the present work, commercial HTG ZnO single crystals of 10×10×0.5 $mm^3$ dimensions, purchased from MaTecK GmbH, were investigated. The crystals were O-terminated with the (0001) orientation. All their surfaces were optically polished. First, the PAS as well as optical measurements were carried out on the as-grown (virgin) crystals. Then, one face of crystals (denoted below as the front side) was subjected to irradiations. The irradiation by 2.5 MeV protons was performed to a fluence of $10^{16}$ $cm^{-2}$ using the Tandetron accelerator at NPI Řež. Other series of ZnO crystals were irradiated with 167 MeV $Xe^{26+}$ ions to fluences of $3\times10^{12}$, $3\times10^{13}$ and $1\times10^{14}$ $cm^{-2}$. The Xe ion irradiations were made at IC-100 FLNR cyclotron in JINR Dubna. Target temperatures during the proton and Xe irradiations, respectively, did not exceed 100 and 50 °C.

### *2.2. Conventional PAS methods*

Involving the conventional PAS techniques in the investigation of Xe irradiated crystals needs in some substantiation. To get an idea of a depth damaged by the irradiation with Xe ions and protons, the depth profiles of implanted Xe ions, protons and irradiation induced vacancies in ZnO were simulated using the SRIM code [12]. The results of SRIM simulations for the 167 MeV Xe ions and 2.5 MeV protons were plotted against the penetration depth in the ZnO single crystal in figure 1. The stopping profile of $^{22}Na$ $\beta^+$ particles in ZnO, characterised by the mean penetration depth of $z_0 \approx 48$ μm, is also given in the figure for comparison. It is suggested by the data of figure 1 that irradiation damaged regions edge at depths of ≈ 40 and 12 μm, respectively, for protons and Xe ions. Considerable portions of $q \approx 57$ and 21 % of $^{22}Na$ positrons, respectively, are stopped within damaged regions making thus the conventional PAS to be efficient method in both cases of 2.5 MeV proton and 167 MeV Xe ion irradiations of bulk ZnO single crystals. On the other hand, the conventional PAS can provide only

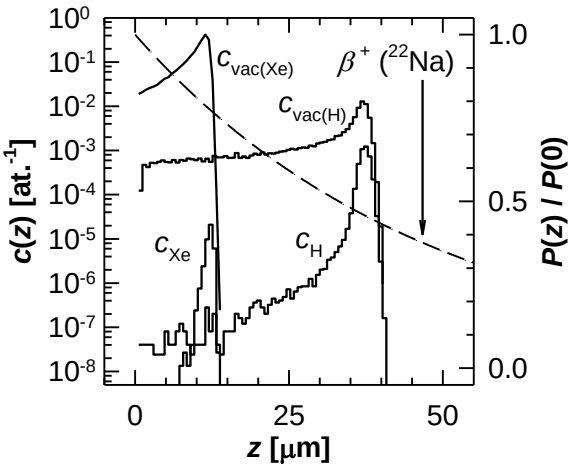


**Figure 1.** Solid line histograms (the left vertical scale) – the SRIM simulated depth profiles plotted against depth $z$ in ZnO single crystal: 2.5 MeV protons ($c_H$), 167 MeV Xe ions ($c_{Xe}$) and vacancies ($c_{vac(H)}$ and $c_{vac(Xe)}$, respectively) created by proton and Xe irradiations.
Dashed line (the right vertical scale) – the stopping profile $P(z)$ of $^{22}$Na positrons in ZnO single crystal normalised to its surface value at $z = 0$.

information integrated over a thickness of damaged layer without any sensitivity to the damage depth profile.

Positron sources for the conventional LT and CDB measurements consisted of ≈ 1 MBq of carrier-free $^{22}$Na carbonate activity (iThembaLABS production) sealed between 2 μm Mylar® C (Dupont) bearing and covering foils. The source was tightly sandwiched between two identical pieces of samples. In selected cases, both of the front, *i.e.* irradiated, and the rear, *i.e.* unirradiated sides of samples were probed by positrons. The conventional PAS measurements were conducted in air at room temperature.

LT spectra were measured by means of a digital delayed-coincidence spectrometer [13] equipped with $BaF_2$ scintillators. The spectrometer exhibited a time resolution of 145 ps (FWHM for $^{22}$Na energy windows). At least $10^7$ coincidence events were collected in each LT spectrum. Measured LT spectra were decomposed into discrete exponential components using a code [14] maximizing the likelihood function. Contribution of annihilations from positron source was derived on the basis of reference LT measurements with a well-annealed $\alpha$-Fe sample with intensity recalculation for ZnO according to a procedure suggested in [15].

CDB spectra were acquired using a digital HPGe–HPGe coincidence spectrometer [16] exhibiting an energy resolution of 0.9 keV (FWHM in coincidence mode at 511 keV $\gamma$-ray energy). Each two-dimensional (2D) energy spectrum contained at least $10^8$ coincidence events. The one-dimensional Doppler-broadened profiles (DBPs) were then extracted from the 2D spectra and displayed as the ratios to the DBP shown by a well-annealed pure Al specimen. A peak-to-background ratio observed for DBPs was better than $10^5$. In addition, the CDB spectra for the well-annealed high-purity zinc metal and alumina ($Al_2O_3$) were taken for sake of comparisons.

### *2.3. SPIS measurements*

SPIS measurements were performed using a magnetically guided variable-energy slow-positron beam SPONSOR [17]. The energies of incident monoenergetic positrons covered a range from 30 eV to 35 keV corresponding to a mean penetration depth of positrons in ZnO ranging from the surface up to 2.3 μm. The DB shape of the 511 keV annihilation peak was measured with a HPGe $\gamma$-spectrometer exhibiting an energy resolution of 1.09 keV (FWHM) at this energy. Typically, ≈ $5\times10^5$ counts were collected in the 511 keV peak. The DB peak shapes were characterised by the ordinary sharpness ($S$) and wing ($W$) parameters [18] evaluated as functions of positron energy $E_+$.

### *2.4. Optical methods*

An UV-VIS spectrometer (Ocean Optics) equipped with a deuterium tungsten halogen light source and a grating monochromator was employed in OT measurements. The measurements were conducted at room temperature within a wavelength interval from 340 through 880 nm. To a first approximation,

the reflectivity of each crystal was considered to be independent of wavelength so that no corrections of the transmitted light intensity for reflectivity variations with wavelength were applied.

PL apparatus was composed of an Olympus IX-71 inverted microscope with an Ealing 25×/0.4 mirror objective and an ARC SP-2300i imaging spectrometer. Samples were irradiated by an UV LED lamp generating 325 or 310 nm photons. A LN-cooled back-illuminated CCD was used to detect luminescence. A lateral resolution of ≈ 0.5 μm was exhibited by the imaging system. The PL spectra were measured at room temperature.

## 3. Results and discussion

In table 1, positron lifetimes $\tau_i$ and relative intensities $I_i$ of exponential components, recognised in the measured LT spectra as arising from positron annihilations in ZnO samples, are shown (i = 2,3,4). Not shown were two weak components that originated from annihilations in the positron source exhibiting lifetimes (intensities) 368 ps (9 %) and 1.8 ns (2 %).

**Table 1.** Positron lifetimes $\tau_i$ and relative intensities $I_i$ (i=2,3,4) of exponential components resolved in the LT spectra of ZnO. Fluences *f* are shown in the second column, in which symbols 'r' indicate measurements of the rear side of irradiated samples. The intensities are normalised so that $\sum_i I_i = 100$ %. The standard deviations are given in parentheses in the units of the last significant digit.

| ZnO sample | $f$ [cm$^{-2}$] | $\tau_2$ [ps] | $I_2$ [%] | $\tau_3$ [ps] | $I_3$ [%] | $\tau_4$ [ps] | $I_4$ [%] |
|---|---|---|---|---|---|---|---|
| virgin | | 183.2 (1) | 100 | | | | |
| $Xe^{26+}$ irrad. | $3\times10^{12}$ | 184 (1) | 86.3 (8) | | | 369.6(6) | 13.7(7) |
| | $3\times10^{13}$ | 185.4 (5) | 78.9 (4) | | | 365(2) | 21.1(5) |
| | $1\times10^{14}$ | 184.1 (7) | 74.5 (8) | | | 351(1) | 25.5(7) |
| | r $1\times10^{14}$ | 183 (2) | 100 | | | | |
| $H^+$ irrad. | $1\times10^{16}$ | 175 (5) | 71 (2) | 260 (2) | 29 (2) | | |
| | r $1\times10^{16}$ | 180 (1) | 100 | | | | |

In all the samples of table 1, the shortest observed lifetime $\tau_2$ appeared to exhibit a value around 182 ps. In the virgin ZnO as well as in both irradiated samples faced to the positron source by their rear side, $\tau_2$-component was the only component arising from annihilations in ZnO crystal. When the irradiated ZnO samples were faced to the source by their front side, an additional component with lifetime $\tau_3 \approx 260$ ps and $\tau_4 \approx 360$ ps, respectively, appeared for the proton and Xe ion implanted samples, representing thus a purely irradiation-induced effect.

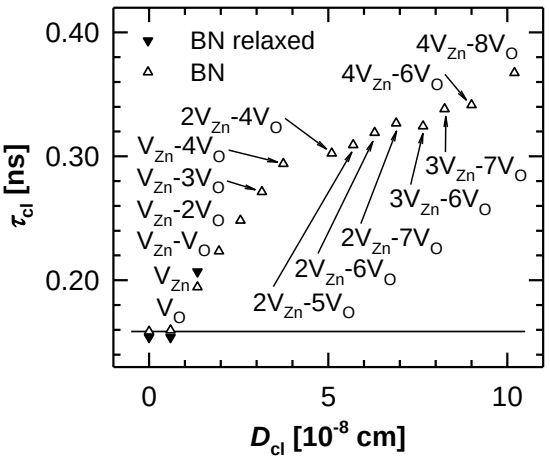


**Figure 2.** Calculated positron lifetimes $\tau_{cl}$ for selected vacancy clusters in ZnO plotted against cluster size $D_{cl}$ (see the text for further details).

There was a long-lasting debate about lifetime $\tau_B$ exhibited by delocalised positrons in the perfect zinc oxide lattice. Several authors [5,18] claimed that $\tau_B \approx 150$ ps while some others [3] stated $\tau_B$ to be as high as ≈ 180 ps. Comprehensive treatment of these discrepancies, taking into account all available experimental as well as theoretical data, was undertaken by Brauer et al. [9]. Based on their argumentation, we adopt the lifetime of delocalised positrons in the perfect ZnO lattice to be $\tau_B \approx 152$ ps. Since positron lifetimes given in table 1 significantly exceed this $\tau_B$-value, their origin has fully to come from saturated positron trapping in defects, *i.e.* no components

corresponding to delocalised positrons ($\tau_1$) could be observed. The present $\tau_2$-components undoubtedly arise from annihilations of positrons trapped in the grown-in $V_{Zn}$–1H complexes which were clearly proven earlier to exist in the HTG ZnO crystals [9,11]. The $\tau_3$-value observed in the proton irradiated sample, see table 1, appears to be close to the lifetime ≈ 260 ps observed in [5] in the 10 MeV electron irradiated ZnO and attributed there to positron trapping in the irradiation-induced $V_{Zn}$–$V_O$ divacancies. Because damage induced by 2.5 MeV protons is expected to be similar to that produced by 10 MeV electrons, it is natural to assign the present proton-induced $\tau_3$-component to positrons trapped in $V_{Zn}$–$V_O$ divacancies, too.

The $\tau_4$-lifetime of ≈ 360 ps resulting from $Xe^{26+}$ irradiations (see table 1) obviously belongs to positron trapping in larger open-volume defects. To estimate their size, a variety of selected agglomerates of vacancy-like defects, composed of $m$ zinc vacancies and $n$ oxygen vacancies, $mV_{Zn}$–$nV_O$, was modelled and respective positron lifetimes were calculated by *ab-initio* calculations using the atomic superposition (ATSUP) method [19]. The electron-positron correlation has been included within the Boroński-Nieminen (BN) approach with the correction for incomplete positron screening taking the high-frequency dielectric constant as $\varepsilon_\infty = 4$ [20]. In figure 2, the positron lifetimes calculated for various vacancy-like agglomerates $mV_{Zn}$–$nV_O$ were plotted against agglomerate size parameter $D_{cl}$ introduced as a diameter of a sphere which volume is equivalent to a sum of volumes of $m$ $V_{Zn}$ and $n$ $V_O$ monovacancies. The data of figure 2 suggest that observed $\tau_4$-lifetimes best correspond to vacancy agglomerates of open volume equivalent to ≈ 10 to 12 monovacancies.

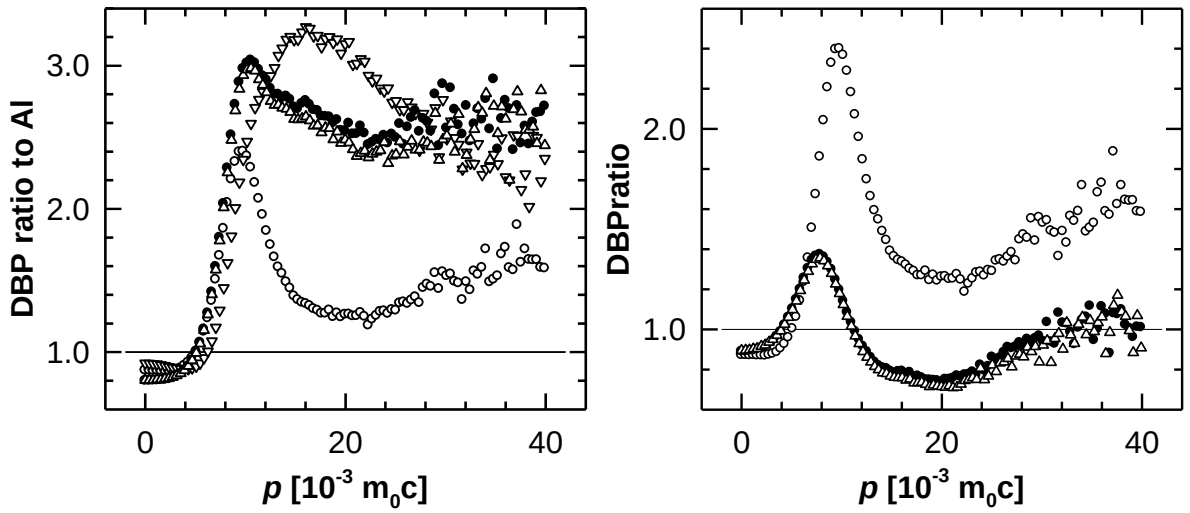


**Figure 3.** DBP ratios plotted as functions of electron momentum $p$ : , ● – virgin ZnO crystal, Δ – Xe irradiated ZnO crystal ($1\times10^{14}$ cm$^{-2}$), ○ – $Al_2O_3$ , ∇ – pure zinc metal. The left panel: All the DBPs are related to well-annealed pure Al metal. The right panel: $Al_2O_3$ is related to well-annealed pure Al metal (as in the left panel), but virgin as well as irradiated ZnO are related to well-annealed pure Zn metal.

The present CDB results are displayed as the DBP ratios to a well-annealed pure Al or Zn metals in figure 3 where they are compared to the DBP ratios measured for the high purity zinc metal and alumina ($Al_2O_3$). Note that DBP ratio for $Al_2O_3$ with respect to Al is expected to exhibit merely a contribution which is characteristic of 2p oxygen electrons in a similar way as the ratio curve for SiO2 with respect to Si [21]. The figure thus suggests that a dominating effect observed in the CDB spectra of ZnO samples comes from oxygen 2p electrons.

The SPIS results of the present work are shown in figure 4. The measured $S$-parameters of the figure were fitted with the VEPFIT code [22] giving the positron diffusion lengths collected in table 2. Combination of the SPIS and LT results can be utilised to estimate the concentrations of irradiation

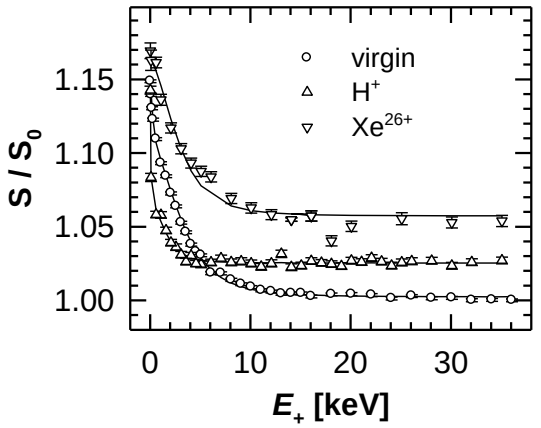


**Figure 4.** Measured *S*-parameters as functions of positron energy $E_+$. Solid lines represent VEPFIT calculations. The *S*-values are normalised to the fitted bulk *S*-parameter for virgin ZnO, $S_0 = 0.5004$.

**Table 2.** VEPFIT evaluations of SPIS data: $L_+$ – positron diffusion length, $S_{bulk}/S_0$ – bulk *S*-parameter normalized to that of virgin ZnO.

| sample | $f$ [cm$^{-2}$] | $L_+$ [nm] | $S_{bulk}/S_0$ |
|---|---|---|---|
| virgin | | 58 ± 2 | 1.0000 |
| $Xe^{26+}$ irrad. | $1\times10^{14}$ | 47 ± 2 | 1.0574±0.0007 |
| $H^+$ irrad. | $1\times10^{16}$ | 19 ± 2 | 1.0253±0.0007 |

induced defects. First, the concentration $c_{V_{Zn}-1H}$ of the $V_{Zn}$–1H defect in the virgin ZnO can be estimated from the measured positron diffusion length $L_+$ of table 2 using the expression [22]

$$c_{V_{Zn}-1H} = \frac{1}{\mu_{V_{Zn}-1H}\,\tau_B}\left(\frac{L_{+,B}^2}{L_+^2} - 1\right), \qquad (1)$$

where $L_{+,B}$ and $\tau_B$ denote the positron diffusion length and lifetime in a perfect zinc oxide lattice, respectively, and $\mu_{V_{Zn}-1H}$ is the positron specific trapping rate for the $V_{Zn-1H}$ defect. Inserting into eq. 1 $\tau_B \approx 152$ ps [9] and the values typical for semiconductors [23], viz.

$$L_{+,B} \approx 200 \text{ nm and } \mu_{V_{Zn}-1H} \approx 1\times10^{15} \text{ s}^{-1},$$

the $c_{V_{Zn}-1H}$ is estimated as $\approx 7\times10^{-5}$ at.$^{-1}$. Then the concentration $c_{cl}$ of the Xe irradiation induced clusters can be estimated within the simple trapping model [24] as

$$c_{cl} = \frac{1}{q}\frac{I_4}{I_2}\frac{\Omega_{V_{Zn}-1H}}{\Omega_{cl}}\mu_{V_{Zn}-1H}\,c_{V_{Zn}-1H}. \qquad (2)$$

In this equation, $\Omega_{V_{Zn}-1H}$ and $\Omega_{cl}$ stand for volumes of the $V_{Zn-1H}$ and cluster, respectively, $\Omega_{cl}/\Omega_{V_{Zn}-1H} \approx \Omega_{4V_{Zn}-8V_O}/\Omega_{V_{Zn}-1H} \approx 4.7$. Factor $q$ accounts for a fraction of positrons that are stopped within the depth damaged by Xe ions. The concentration $c_{cl}$ of Xe ions induced clusters, estimated using eq. 2 with $q \approx 0.2$ indicated by the above SRIM simulations, was plotted in figure 5 against the Xe ion fluence. One can notice in the figure a trend to a plateau-like pattern displayed by $c_{cl}$-values when the fluence increases to $\approx 1\times10^{14}$ cm$^{-2}$. An overlapping of Xe ion tracks may lie behind the cluster creation.

Measured transmittances $T$ are represented as functions of wavelength $\lambda$ in figure 6. For the virgin ZnO crystal, $T$-curve exhibits a shape which is essentially the same as that reported earlier for HTG ZnO single crystals [25]. A rapid onset of $T$ occurs at $\lambda \approx 390$ nm with $T$ risen up to $T \approx 60$ % at $\lambda \approx 410$ nm. Then the slope of $T$ is gradually dropped down and finally a very slow and almost linear increase of $T$ with increasing $\lambda$ is observed above $\lambda \approx 550$ nm, reaching a maximum value of $T \approx 80$ % at $\lambda \approx 880$ nm.

For the proton-implanted ZnO crystal, the observed transmittance closely follows that found for the virgin crystal, except for the 400 to 550 nm wavelength range (figure 6). At $\lambda \approx 400$ nm ($T \approx 25$ %), the observed transmittance in the proton-implanted ZnO becomes significantly reduced with respect to the virgin crystal, growing roughly linearly up to a value of $T \approx 75$ % at $\lambda \approx 550$ nm, i.e.

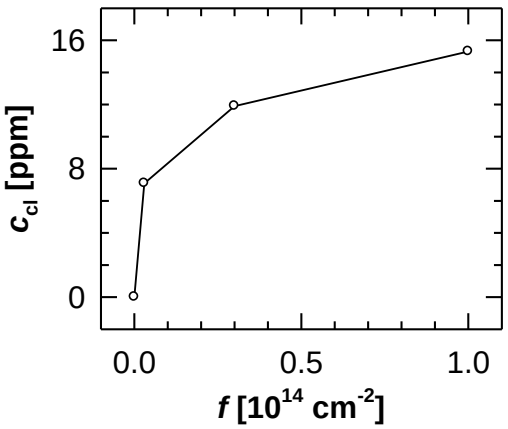


**Figure 5.** Estimated concentrations $c_{cl}$ of Xe ion irradiation induced clusters in ZnO vs Xe ion fluence $f$.

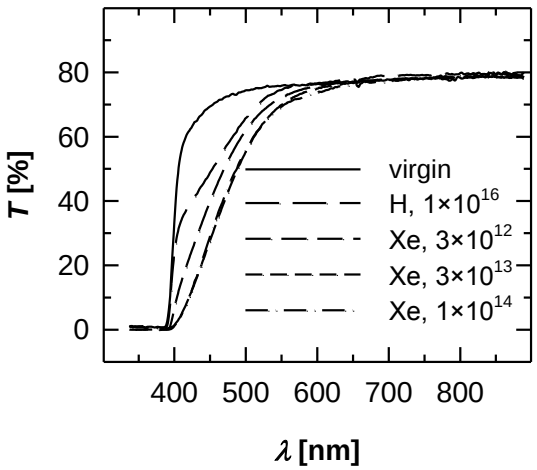


**Figure 6.** Measured transmittances $T$ as functions of wavelength $\lambda$.

reaching again a $T$-values found in the virgin ZnO (see figure 6). Thus defects which are optically active in the violet – blue – green spectral region are brought into the ZnO crystals by 2.5 MeV proton irradiation. Protons of such relatively low energy are capable to produce only atomic size defects ($V_{Zn}$ or $V_O$, interstitials, divacancies) in the subsurface layer of ≈ 40 μm depth of ZnO crystals. It is obvious that some of these point defect types should be regarded as a cause of the observed suppression of transmittance within a 410 to 550 nm region. Of them, however, only $V_{Zn}$ and $V_{Zn}$–$V_O$ defects could be detected by PAS and $V_{Zn}$–$V_O$ defects were indeed observed in proton irradiated ZnO crystal, see table 1.

In the Xe-implanted ZnO crystals, irradiation-induced suppression of transmittance inside a 410 to 550 nm region is even more pronounced than in the proton-implanted sample. Transmittance is further reduced for a fluence of $f \approx 3\times10^{13}$ cm$^{-2}$ compared to that of $f \approx 3\times10^{12}$ cm$^{-2}$, see figure 6, showing on the other hand a plateau effect at a fluence of $\approx 1\times10^{14}$ cm$^{-2}$. Note that an approaching to a plateau is also seen in cluster concentration data discussed in the preceding text. Vacancy clusters created inside a 12 μm subsurface layer by Xe ion irradiation of ZnO crystals should be considered as a likely cause of observed transmittance dropping down in this case.

The PL spectra taken for the virgin and implanted ZnO crystals are displayed as functions of wavelength $\lambda$ in figure 7. A green emission (GE) band with a broad maximum at $\lambda \approx 550$ nm [1] is clearly seen for the virgin ZnO crystal. For both irradiation species, however, the GE becomes completely suppressed to a level of scattering background of the spectrometer. Despite of a great volume of research work, the nature of GE band in ZnO remains still not fully understood [26]. Nonetheless, the present PL experiments have suggested that the observed GE quenching is likely a consequence of irradiation induced defects of sufficient concentrations providing a channel for dominating non-radiative recombination of charge carriers.

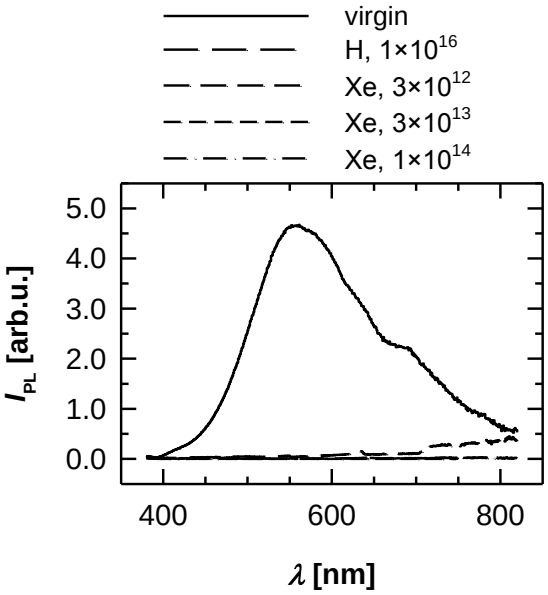


**Figure 7.** PL intensity $I_{PL}$ plotted as function of wavelength $\lambda$.

## 4. Conclusions

In the present work, hydrothermally grown bulk ZnO single crystals were implanted with the 2.5 MeV protons to a fluence of $1\times10^{16}$ cm$^{-2}$ and the 167 MeV $Xe^{26+}$ ions to fluences of $3\times10^{12}$, $3\times10^{13}$ and $1\times10^{14}$ cm$^{-2}$. Irradiation induced changes were studied by means positron annihilation techniques (positron lifetime, coincidence Doppler broadening and slow-positron implantation spectroscopy measurements) combined with optical methods (optical transmittance, photoluminescence). The PAS results were correlated with those obtained by the optical methods.

The grown in as well as irradiation induced defects in ZnO crystals were characterised: the grown in $V_{Zn}$–1H complexes, the $V_{Zn}$–$V_O$ divacancies created in the proton irradiated crystals, and the larger defects of size comparable to clusters of ≈ 10 to 12 vacancies identified in the Xe implanted crystals. Concentrations of the observed defects were estimated by combining LT and SPIS results. The irradiation induced defects were demonstrated to be optically active in the 400 to 550 nm wavelength region. The green emission band which is well-seen in the virgin ZnO crystal was completely destroyed in the both proton and Xe ion irradiated samples which may be likely connected with irradiation-induced channels for non-radiation recombination of charge carriers.

Trend to a plateau-like behaviour of irradiation induced changes at a Xe ion fluence of $\approx 1\times10^{14}$ cm$^{-2}$, exhibited by the present OT data as well as cluster concentration estimates, may be tentatively regarded as an evidence of strongly overlapping heavy ion tracks at sufficiently high fluences when no additional increase of structure disorder in the damaged subsurface layer can obviously be produced by increasing fluence. Similar considerations have recently been reported for heavy ion implanted sapphire crystals [27]. Indeed, further studies of these interesting phenomena may be of a significant theoretical as well as practical interest.

**Acknowledgements**
Present investigation was financially supported by the Czech Science Foundation under the project P108/11/0958. Also financial support of the cooperation of the Czech Republic with JINR within the '3+3' project is highly acknowledged.

**References**

[1] Özgür Ü, Alivov Ya I, Liu C, Teke A, Reshchikov M A, Doğan S, Avrutin V, Cho S-J and Morkoç H 2005 *J. Appl. Phys.* **98** 041301
[2] Ursaki V V, Rusu E V, Sarua A, Kuball M, Stratan G I, Burlacu A and Tiginyanu I M 2007 *Nanotechnology* **18** 215705
[3] Tuomisto F, Ranki V, Saarinen K and Look D C 2003 *Phys. Rev. Lett.* **91** 205502
Tuomisto F, Saarinen K, Look D C and Farlow G C 2005 *Phys. Rev.* B **72** 085206
[4] Brunner S, Puff W, Balogh A G and Mascher P 2001 *Mater. Sci. Forum* **363–365** 141
[5] Brauer G, Anwand W, Skorupa W, Kuriplach J, Melikhova O, Moisson C, von Wenckstern H, Schmidt H, Lorenz M and Grundmann M 2006 *Phys. Rev.* B **74** 045208
[6] Ronning C, Gao P X, Ding Y, Wang Z L and Schwen S 2004 *Appl. Phys. Lett.* **84** 783
[7] Regel' V P, Nikitenko V A, Kuzmina I P, Galstyan V G, Dolukhanyan T P, Nikul'shin S F, Sizova N L and Skuratov V A 1987 *Sov. Phys. – Tech. Phys.* **32** 183
[8] Burlacu A, Ursaki V V, Skuratov V A, Lincot D, Pauporte T, Elbelghitt T, Rusu E V and Tiginyanu I M 2008 *Nanotechnology* **19** 215714
[9] Brauer G, Anwand W, Grambole D, Grenzer J, Skorupa W, Čížek J, Kuriplach J, Procházka I, Ling C C, So C K, Schulz D and Klimm D 2009 *Phys. Rev.* B **79** 115201
[10] Van de Walle C G 2001 *Physica B* **308–310** 899
[11] Cizek J, Zaludova N, Vlach M, Danis S, Kuriplach J, Prochazka I, Brauer G, Anwand W, Grambole D, Skorupa W, Gemma R, Kirchheim R and Pundt A 2008 *J. Appl. Phys.* **103** 053508
[12] Ziegler J F, Ziegler M D and Biersack J P 2010 *Nucl. Instr. Meth in Phys. Research* B **268** 1818 Information on www.srim.org
[13] Becvar F, Cizek J, Prochazka I and Janotova J 2005 *Nucl. Instr. Meth. in Phys. Research* A **539** 372
[14] Prochazka I, Novotny I and Becvar F 1997 *Mater. Sci. Forum* **255–257** 772
[15] Surbeck H 1977 *Helv. Phys. Acta* **50** 705
[16] Cizek J, Vlcek M and Prochazka I 2010 *Nucl. Instr. Meth. in Phys. Research* A **623** 982
[17] Anwand W, Brauer G, Butterling M, Kissener H R and Wagner A 2012 *Defects and Diffusion Forum* **331** 25

[18] Mizuno M, Araki H and Shirai Y 2004 *Materials Transactions* **45** 1964
[19] Puska M J and Nieminen R M 1983 *J. Phys.* F **13** 333
Seitsonen A P, Puska M J and Nieminen R M 1995 *Phys. Rev.* B **51** 14057
[20] Boronski E and Nieminen R M 1986 *Phys. Rev.* B **34** 3820
Puska M J, Mäkinen S, Manninen M and Nieminen R M 1989 *Phys. Rev.* B **39** 7666
[21] Brusa R S, Deng W, Karwasz G P, Zecca A and Pliszka D 2001 *Appl. Phys. Lett.* **79** 1492
[22] Van Veen A, Schut H, Clement M, de Nijs J M M, Kruseman A and IJpma M 1995 *Appl. Surf. Sci.* **85** 216
Van Veen A, Schut H, de Vries J, Hakvoort R A and IJpma M R 1990 *AIP Conf. Proc.* **218** 171
[23] Krause-Rehberg R and Leipner H S 1999 *Positron Annihilation in Semiconductors – Defect Studies* (Berlin: Springer)
[24] West R N 1979 *Positrons in Solids* ed P Hautojärvi (Berlin: Springer-Verlag) p 89
[25] Anwand W, Brauer G, Grynszpan R I, Cowan T E, Schulz D, Klimm D, Cizek J, Kuriplach J, Prochazka I, Ling C C, Djurisic A B, Klemm V, Schreiber G and Rafaja D 2011 *J. Appl. Phys.* **109** 063516
[26] Sun Y, Guo H, Jiang F, Yuan R, Zhang J, Zeng X, Zhou T, Qiu Y, Zhang B, Xu K and Yang H, 2013 *Appl. Surf. Sci.* **283** 258
[27] Liszkay L, Gordo P M, Havancsak K, Skuratov V A, de Lima A and Kajcsos Zs 2004 *Mater. Sci. Forum* **445–446** 138